A 'warm path' for Gulf Stream–troposphere interactions

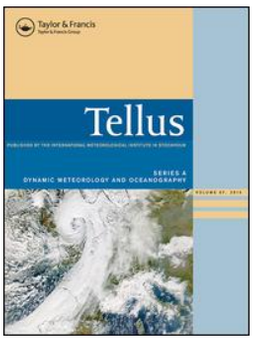

Tellus A: Dynamic Meteorology and Oceanography

ISSN: (Print) 1600-0870 (Online) Journal homepage: http://www.tandfonline.com/loi/zela20

A 'warm path' for Gulf Stream–troposphere interactions

Luke Sheldon, Arnaud Czaja, Benoit Vannière, Cyril Morcrette, Benoit Sohet, Mathieu Casado & Doug Smith

To cite this article: Luke Sheldon, Arnaud Czaja, Benoit Vannière, Cyril Morcrette, Benoit Sohet, Mathieu Casado & Doug Smith (2017) A 'warm path' for Gulf Stream–troposphere interactions, Tellus A: Dynamic Meteorology and Oceanography, 69:1, 1299397

To link to this article: http://dx.doi.org/10.1080/16000870.2017.1299397

Tellus
SERIES A
DYANAMIC
METEOROLOGY
AND OCEANOGRAPHY
PUBLISHED BY THE INTERNATIONAL METEOROLOGICAL INSTITUTE IN STOCKHOLM

A 'warm path' for Gulf Stream–troposphere interactions

By LUKE SHELDON[1], ARNAUD CZAJA[1]*, BENOIT VANNIÈRE[2], CYRIL MORCRETTE[3], BENOIT SOHET[1], MATHIEU CASADO[4] and DOUG SMITH[3], [1]*Physics Department, Imperial College, London, UK;* [2]*Department of Meteorology, University of Reading, Reading, UK;* [3]*Met Office, Exeter, UK;* [4]*Laboratoire des Sciences du Climat et de l'Environement, UMR8212, CEA-CNRS-UVSQ/IPSL, Gif-sur-Yvette, France*

(Manuscript received 22 December 2016; in final from 12 January 2017)

ABSTRACT

Warm advection by the Gulf Stream creates a characteristic 'tongue' of warm water leaving a strong imprint on the sea surface temperature (SST) distribution in the western North Atlantic. This study aims at quantifying the climatological impact of this feature on cyclones travelling across this region in winter using a combination of reanalysis data and numerical experiments. It is suggested that the Gulf Stream 'warm tongue' is conducive to enhanced upward motion in cyclones because (i) it helps maintain a high equivalent potential temperature of air parcels at low levels which favors deep ascent in the warm conveyor belt of cyclones and (ii) because the large SST gradients to the north of the warm tongue drive a thermally direct circulation reinforcing and, possibly, destabilizing, the transverse circulation embedded in cyclones. This hypothesis is confirmed by comparing simulations at 12 km resolution from the Met Office Unified Model forced with realistic SST distribution to simulations with an SST distribution from which the Gulf Stream warm tongue was artificially removed or made colder by 3 °C. It is also supported by a dynamical diagnostic applied to the ERA interim data-set over the wintertime period (1979–2012). The mechanism of oceanic forcing highlighted in this study is associated with near thermal equilibration of low level air masses with SST in the warm sector of cyclones passing over the Gulf Stream warm tongue, which is in sharp contrast to what occurs in their cold sector. It is suggested that this 'warm path' for the climatic impact of the Gulf Stream on the North Atlantic storm-track is not currently represented in climate models because of their coarse horizontal resolution.

Keywords: ocean–atmosphere interactions, Gulf Stream, climate dynamics

1. Introduction

The meridional overturning circulation and the horizontal gyres of the North Atlantic ocean leave sharp features in its sea surface temperature (SST) distribution. In addition to the general surface warming of the North Atlantic compared to the North Pacific (e.g. Manabe and Stouffer, 1988), the Florida Current and the separated Gulf Stream create a strong deformation of the sea surface isotherms, bringing poleward and eastward a 'tongue' of warm water (see the shape of the 22 °C isotherm in Fig. 1a).[1] To the north of this feature, strong SST gradients are seen while to the south, the wrapping of the SST contours by the Gulf Stream recirculation and the action of mesoscale eddies tend to erode those gradients. In this study, we propose a new pathway through which these features impact the tropospheric circulation in the North Atlantic. In terms of the coupled atmosphere/Atlantic ocean system, this study thus focuses on the ocean → atmosphere pathway rather than on the atmospheric forcing of the Atlantic ocean circulation.

The impact of the warm tongue of the Gulf Stream on air–sea interactions has been highlighted in many studies, in particular its role in setting a region of large net surface heating of the atmosphere, especially in winter (e.g. Gill, 1982; Shaman et al., 2010). At this time of year, extra-tropical cyclones travelling from North America to the Atlantic ocean bring cold dry air of continental origin over the Gulf Stream warm tongue, leading to very large (in excess of hundreds of Wm^{-2}) sensible and latent heat fluxes at the air–sea interface. The impact of the warm tongue above the marine boundary layer has traditionally been understood as a response to these large fluxes and their associated shallow heating of the troposphere (Hoskins and Karoly, 1981; Kushnir et al., 2002).

The discussion above relates to the cold sector of cyclones, where the surface flow is from the north-west, but the presence of the Gulf Stream warm tongue can also influence the

*Corresponding author. e-mail: a.czaja@imperial.ac.uk

Citation: Tellus A: 2017, **69**, 1299397, http://dx.doi.org/10.1080/16000870.2017.1299397

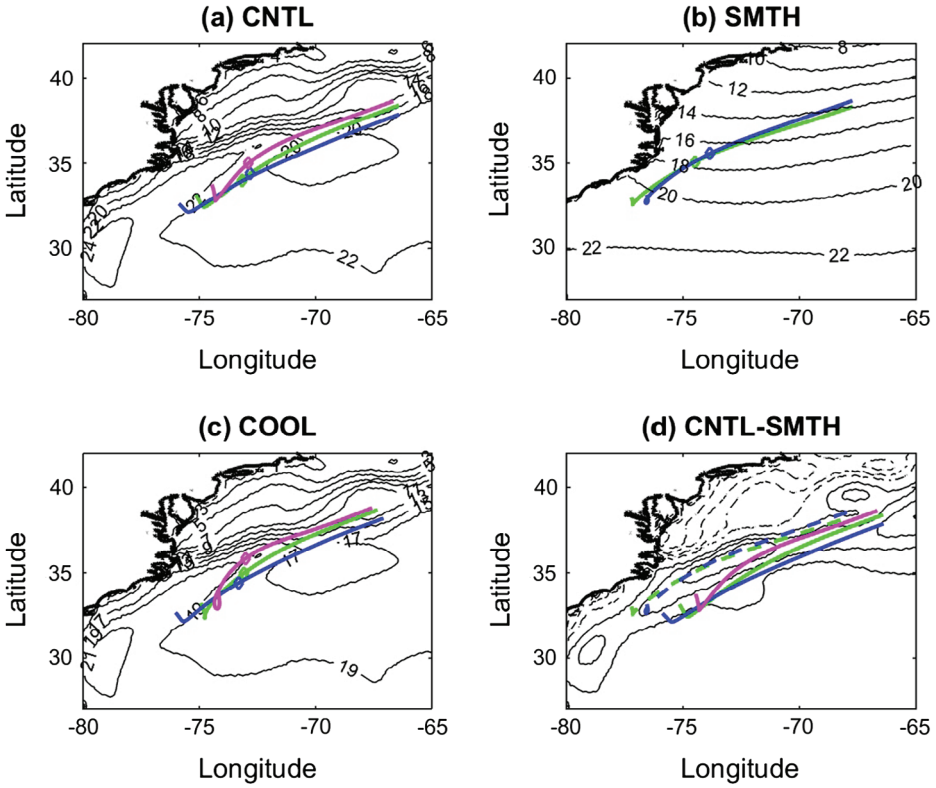

Fig. 1. SST (contoured every 2 °C) used in experiment (a) CNTL (b) SMTH and (c) COOL. Panel (d) gives the difference CNTL-SMTH (contoured every 1.5 °C, positive continuous, negative dashed). The colour curves in panels (a), (b) and (c) are the average horizontal trajectories for the respective experiments, as discussed in Section 2.2 (magenta: $z_o \geq 7$ km, green: 5 km $\leq z_o < 7$ km, blue: $z_o < 5$ km). The diamonds on these curves indicate the average locations when parcels leave the boundary layer. The colour curves in (d) indicate the CNTL (continuous lines) and SMTH (dashed lines) mean trajectories, reproduced from panel (a) and (b), respectively.

atmosphere in their warm sector, where the surface flow is from the south-west. Indeed, the warm sector is where air masses of low-latitude origins are advected poleward and upward, in a manner sometimes referred to as a 'warm conveyor belt' (WCB, see e.g. Browning, 1990). This motion is associated with weak turbulent heat fluxes at the sea surface, even possibly directed downward (e.g. Boutle et al., 2011), but it leads to a deep heating of the troposphere through latent heat release (Hoskins and Valdes, 1990). To focus in this study on the warm sector, we simulate the response of an extra-tropical cyclone to different SST configurations in the western North Atlantic, with and without the Gulf Stream warm tongue, and focus on the induced changes in upward motion (Section 2). These simulations are carried out at high spatial resolution (12 km, i.e. 'high' in the context of global climate models) because it is known that frontal circulations, where the upward motion is concentrated, are too weak in coarse resolution models (e.g. Bauer and Del Genio, 2006; Catto et al., 2010; Willison et al., 2013). In Section 3, we apply a dynamical diagnostic to atmospheric reanalyses data during the wintertime to assess the relevance of the mechanisms discussed in Section 2 to the climatology. A summary and a discussion are offered in Section 4.

2. Experiments with the Met Office Unified Model

2.1. Model set-up

The Met Office Unified Model (hereafter MetUM) has been run in a global configuration on a global grid of horizontal resolution 0.37° × 0.56° (≈ 40 km) to generate the boundary conditions of a North Atlantic domain (using a grid length of ≈ 12 km) being run as a one-way-nested limited area model.[2] The MetUM is a finite difference model which solves the non-hydrostatic, deep-atmosphere dynamical equations. The parameterizations of physical processes include longwave and shortwave radiation, boundary layer mixing, convection and cloud cover and large-scale precipitation. Specifically, we ran the version MetUM 7.3, with the set up used in Martinez-Alvarado et al. (2014). The reader is referred to this paper for details about the model.

The model was initialized on 14 January 2004 at 1200 UTC and integrated over 72 h, using initial conditions from the ECMWF operational analysis. On 15 January 1200 UTC (i.e. 24 h into the simulation), a large tropopause trough was centred on the east coast of North America. The upper level cyclone was associated with a low-level cyclone in the Gulf Stream basin

with lowest pressure equal to 988 hPa. The low-level cyclone deepened by 45 hPa over the course of the following 24 h. We have simulated the passage of this cyclone using three different SST configurations (all constant in time). The first, named CNTL, uses the observed SST distribution on 14 January 2014 at 1200 UTC. The second, named SMTH, uses a smoothed version of the CNTL SST. The smoothing was generated using a spatial filter in which each point is a weighted average of itself and its four immediate neighbours (in the ratio 1:1/4). The filter was applied iteratively 3000 times in a box centred on the Gulf Stream basin with a Gaussian transition to the region outside the box where no smoothing is applied. This experiment is specifically aimed at 'removing' the Gulf Stream warm tongue in order to see its impact on the warm sector of the cyclone. Finally, in a third experiment, named COOL, we lower uniformly the SST by 3 K over the entire nested domain, leaving the SST gradient unaltered. This experiment is carried out to investigate the role of the absolute temperature of the warm tongue, as opposed to the role of the SST gradient north of this feature. All simulations share the same lateral boundary conditions and initial conditions, and differ only by the prescribed SST. The three SST distributions can be compared in Fig. 1 (panels (a), (b), (c) for CNTL, SMTH and COOL, respectively, and panel (d) for the difference CNTL-SMTH).

2.2. *Results*

At 24h into the simulation, a well-defined region of upward motion has developed over the Northwest Atlantic at mid-levels, as indicated by the area with positive upward velocity near 37°N, 68° W in Fig. 2a (red colours). One also notices the presence of another well-developed region of ascent east of 60° W, which is the signature of the previous cyclone having travelled across the Gulf Stream at $t < 0$. Both features are seen in Fig. 2b to be associated with advection of high equivalent potential temperature[3] (θ_e) is at low levels, leading to the characteristic deformation and wrapping of the θ_e contours. One can also notice the alignment of the westernmost high θ_e tongue in Fig. 2b with that of the Gulf Stream warm tongue's signature in the SST field (Fig. 2b, black contours, $CI = 2$ K).

To investigate the differences in the vertical motion field between the CNTL and SMTH experiments, it proved useful to compute back-trajectories starting from the core of the ascent at $t = 24$ h until some of them reach near the sea surface at $t = 0$ h. In doing so, one can investigate how differently the core region of ascent is fed from low level in each experiment. This procedure has the advantage to 'target' the ascending region, unlike in a forward trajectory calculation where the destination of air parcels seeded at low levels is not controlled. More than 70,000 back-trajectories were initialized at $t = 24$ h over the height interval 4 km–8 km (every 100 m) in a region centred on the core of the ascent discussed in the previous paragraph (80° − 60° W, 30° − 45°N). We will refer to this volume as the 'release volume' in the following (shown as a black box in Fig. 3). The back-trajectories were found to split clearly into two distinct families feeding the ascent into the WCB. The first family, representing the vast majority of trajectories, is associated with a gentle ascending motion from the west, crossing over North America (not shown). The second family is associated with air parcels travelling first at low levels over the Gulf Stream before ascending into the free troposphere, and it is this latter set of trajectories which is the focus of our study. (It turns out that these two sets of trajectories could simply be separated depending on whether or not the longitude and latitude of air parcels at $t = 0$ were over the Atlantic ocean – all trajectories over the ocean at $t = 0$ were also found to be at low levels, none of them exceeding an altitude of 1800 m above the sea). Although these are back-trajectories, it is easier to describe them in a 'forward way'. We thus discuss the 'ascent' from $t = 0$ to $t = 24$ h in the remaining of this paper, and we denote the height of air parcels at $t = 24$ h by z_o. We have further decomposed the trajectories in three (color coded)

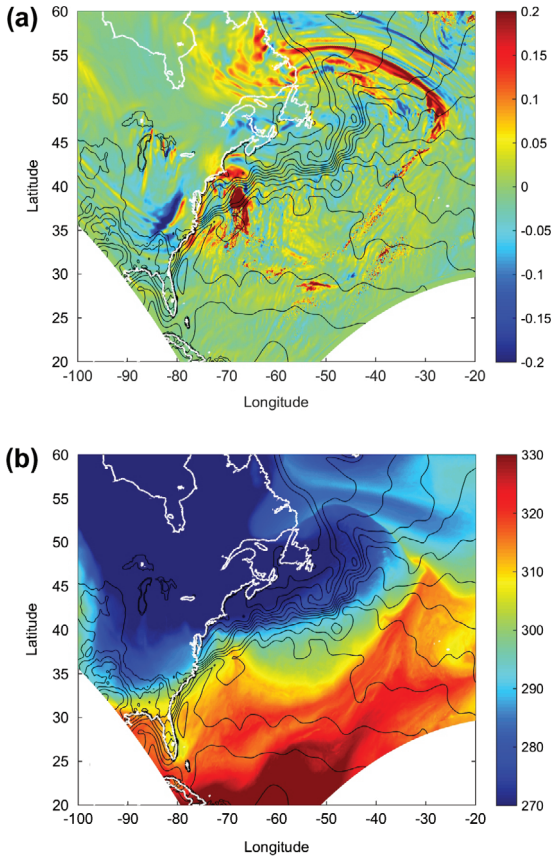

Fig. 2. Snapshots at $t = 24$ h of (a) vertical velocity (w, in m/s) at $z = 5$ km and (b) equivalent potential temperature (θ_e, in K) at $z = 500$ m. The corresponding surface temperature (=SST used in CNTL over the ocean) is shown in black with a contour interval of 2 °C, starting from 0 °C. The 'white corners' indicate the limit of the nested 12 km domain in that particular portion of the Northwest Atlantic.

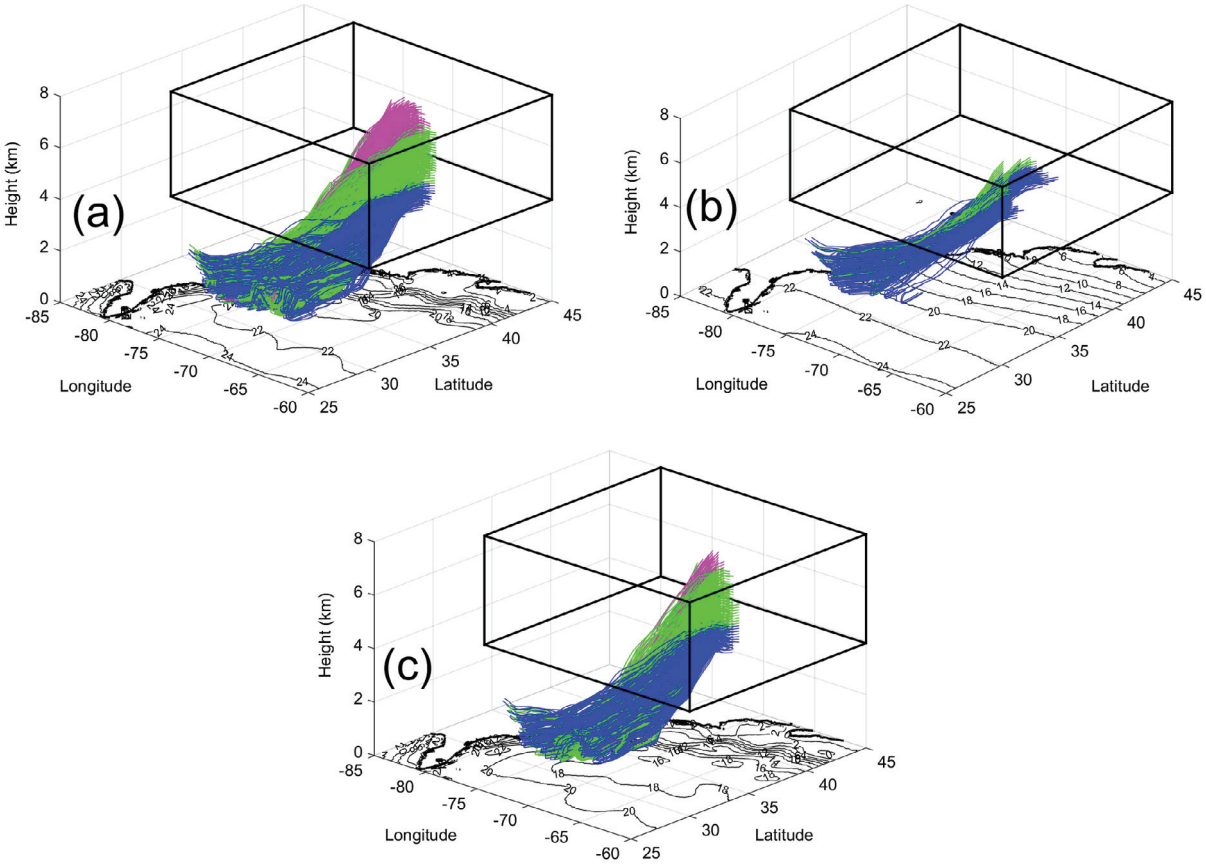

Fig. 3. Back trajectories from the core of ascending motion at $t = 24$ h at mid-levels (the 'release volume' in black) in (a) the CNTL, (b) the SMTH and (c) the COOL experiments. The corresponding SST is shown in black with a contour interval of 2 °C. Note that only trajectories originating from low levels over the ocean at $t = 0$ h are shown. The colour coding refers to different sets of trajectories, depending on the height z_o at $t = 24$ h: $z_o \geq 7$ km (magenta), 5 km $\leq z_o < 7$ km (green) and $z_o < 5$ km (blue).

subsets: $z_o \geq 7$ km (magenta set), 5 km $\leq z_o < 7$ km (green set) and $z_o < 5$ km (blue set).

A three-dimensional view of all trajectories is displayed in Fig. 3. In the CNTL experiment (Fig. 3a), air parcels ascend sharply, reaching all heights encompassed by the release volume (black box). A total of 1178 trajectories fall in this category (Table 1 summarizes the statistics). In contrast, the number for the SMTH experiment (Fig. 3b) is only 275. Not only is there less feeding of the WCB from low levels in the SMTH compared to the CNTL experiment, one can also see that the slope of the ascent is reduced in Fig. 3b compared to Fig. 3a, with parcels reaching only the lowermost part of the release volume by $t = 24$ h. Indeed, only a small subset of the back-trajectories in SMTH have $z_o \geq 5$ km at $t = 24$ h, while these constitute the bulk of the trajectories in CNTL (green and magenta trajectories in Fig. 3a – see also Table 1, 2nd column).

The shape of the trajectories is further explored by comparing the average trajectories (i.e. the mean over all members of a given subset) of each colour subset. Consider first the average height occupied by air parcels throughout the integration (Fig. 4). In both CNTL (Fig. 4a) and SMTH (Fig. 4b), parcels are confined within the boundary layer from $t = 0$ to $t \approx 16$ h (the top of the boundary layer, shown as a dashed line in Fig. 4, was simply estimated from the dry potential temperature (θ) profile by computing the height of the first model layer satisfying $\theta \geq \theta_s + 0.5$ K in which θ_s is θ in the model layer closest to the Earth's surface). It is noticeable that of all subsets, the magenta (i.e. describing parcels reaching to the highest levels) is the one most closely circulating near sea level and the one being the longest time away from the top of the boundary layer, a point to which we will return in the next section. Note that as emphasized above, no parcels were found to reach higher than 7 km in SMTH and hence no magenta curve is displayed in Fig. 4b.

The mean horizontal motion spanned by each subset is shown separately for each experiment in Fig. 1, superimposed on the relevant SST fields (panel (a) for CNTL, (b) for SMTH and (c) for COOL – a diamond indicates the time when the parcel leaves the boundary layer using the curves in Fig. 4). To help

Table 1. Number of back-trajectories feeding the 'release volume' from low levels for the different experiments discussed in the text (rows labelled 'all'). Contributions from different layers are also indicated based on the height z_o of the parcels at $t = 24$ h.

Experiment	12 km	40 km	ratio (40 km/12 km)
CNTL			
(all)	1178	734	0.62
($z_o \geq 7$ km)	167	0	0
(5 km $\leq z_o <$ 7 km)	613	334	0.54
($z_o <$ 5 km)	398	400	1
($z_o \geq 5$ km)/($z_o <$ 5 km)	1.95	0.83	0.42
SMTH			
(all)	275	148	0.53
($z_o \geq 7$ km)	0	0	0
(5 km $\leq z_o <$ 7 km)	27	0	0
($z_o <$ 5 km)	248	148	0.6
($z_o \geq 5$ km)/($z_o <$ 5 km)	0.1	0	0
COOL			
(all)	625	394	0.63
($z_o \geq 7$ km)	29	0	0
(5 km $\leq z_o <$ 7 km)	306	98	0.32
($z_o <$ 5 km)	290	296	1.02
($z_o \geq 5$ km)/($z_o <$ 5 km)	1.15	0.33	0.28

the comparison, the mean horizontal trajectories for CNTL and SMTH are then plotted together in Fig. 1d, keeping the colour coding but using continuous lines for CNTL, and dashed lines for SMTH. The overall direction of the motion is qualitatively similar in all experiments, with a clear north-eastward orientation reflecting the general motion of air masses in the travelling cyclone in which the air streams are embedded. Nevertheless, there is a significant spread among the horizontal trajectories, with the ones in SMTH lying farther to the north-west and the ones in CNTL farther to the south-east.

2.3. *Mechanisms*

2.3.1. 'Thermodynamical' and 'dynamical' mechanisms. The statistics summarized in Table 1, in particular the ratio of number of trajectories with z_o above/below 5 km (last row for each experiment in Table 1), show that the presence of the Gulf Stream warm tongue has a significant impact on the upward motion present in the cyclone and we next attempt to explain what controls this effect. One possible line of thought arises from further consideration of the shape of the air parcels' trajectories at low levels. In the CNTL experiment (Fig. 1a, colour curves), these trajectories are approximately parallel to the Gulf Stream warm tongue, i.e. they remain over a relatively warm and isothermal part of the ocean. It is conceivable that this 'matching' of oceanic and atmospheric flows makes it possible for warm and

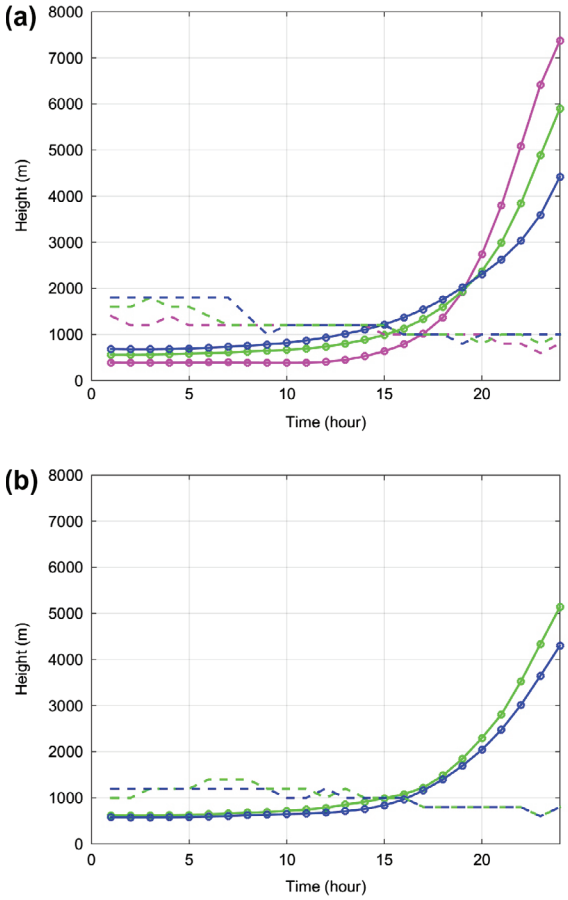

Fig. 4. Evolution of the parcels' height (in m, y-axis) through time (in h, x-axis) for the (a) CNTL and (b) SMTH experiments. The height of the boundary layer is indicated as a dashed line. The colour coding is the same as in Fig. 3.

moist air parcels of low latitude origins to flow over the ocean without significant loss of heat (and also a gain of moisture) and thus maintain high θ_e values. Everything else being equal, this will increase the likelihood of connecting upper and lower levels' high θ_e surfaces into a single frontal surface, leading to vigorous ascent throughout the troposphere (e.g. Pauluis et al., 2010). In contrast, in the SMTH experiment (Fig. 1b), air parcels cross more SST contours while they flow at low levels over the ocean since the Gulf Stream warm tongue is absent, which could conceivably reduce their θ_e and the likelihood of ascent. We refer to this mechanism as the 'thermodynamical' mechanism.

Another possible line of thought, based on the dynamical arguments put forward in Eliassen (1962), is that the presence of stronger SST gradients in the CNTL experiment is driving a thermally direct cell enhancing the frontal circulation present in the cyclone in the first place. As the SST gradients are weakened in SMTH, the net frontal circulation would be reduced, explaining the weaker feeding of the WCB from low levels in

Fig. 3b compared to Fig. 3a. Alternatively, it could also be that the stronger SST gradients in CNTL help destabilize the frontal circulation by enhancing the vertical windshear (a lowering of the Richardson number – see Bennetts and Hoskins, 1979; Czaja and Blunt, 2011). We collectively refer to these scenarios as the 'dynamical mechanism'.

To distinguish between these two broad classes of mechanisms, we analyse the back-trajectories found in the COOL experiment (Fig. 3c), which should preserve the dynamical mechanism (no change in the SST gradients) but should weaken severely the thermodynamic mechanism. Obviously, the smoothing in SMTH not only alters the SST gradient but also the absolute SST values, with a cooling on the geographical location of the warm flank of the Gulf Stream and a warming on its poleward flank. It is for this reason that we chose to lower the SST by 3 K in COOL so that the absolute value of SST in the geographical location of the Gulf Stream warm tongue remains comparable in both experiments (see the SST anomaly corresponding to CNTL-SMTH in Fig. 1d for comparison). As can be seen in Fig. 3c, the COOL experiment is somewhat in between the CNTL and SMTH. A total of 625 back-trajectories were obtained, as opposed to 275 and 1178 in SMTH and CNTL, respectively. Breakdown of the initial heights in each of these experiments in Table 1 (2nd column) indicates that the bulk of the trajectories originates above 5 km in COOL (green and magenta trajectories), as in CNTL, in contrast to SMTH where we saw in Section 2 that the bulk of the trajectories originated from below 5 km. This suggests that the partitioning between bottom or top heavy feeding of the ascent from low levels is primarily set by the SST gradient. In addition, we note that the absolute numbers of trajectories is much reduced in COOL compared to CNTL, with only 29 trajectories originating above 7 km in COOL compared to 167 in CNTL. Thus, the ability of air parcels to ascend in the WCB is sensitive to the absolute SST over the warm tongue, demonstrating an important role for the thermodynamical mechanism.

2.3.2. Thermodynamic analysis. The thermodynamic mechanism is further investigated by following the evolution of the moist equivalent temperature θ_e of parcels while they are in the boundary layer, and thus directly affected by the exchange of heat and moisture with the underlying ocean. According to the thermodynamical mechanism, the SST configuration in CNTL should allow air parcels to leave the boundary layer with relatively high θ_e while this should not happen in SMTH. This idea is tested in Fig. 5, which displays the evolution of (SST, θ_e) while parcels are in the boundary layer. To construct this evolution, we simply estimated the θ_e that a fictitious parcel would have if it followed the average trajectory of a given colour subset. An SST value was given to the fictitious parcel by simply computing the underlying SST at its horizontal location through time. Let us first analyse the situation at $t = 0$ h, identified by a diamond. It is seen that although the range of SST (x-axis) is distinguishable

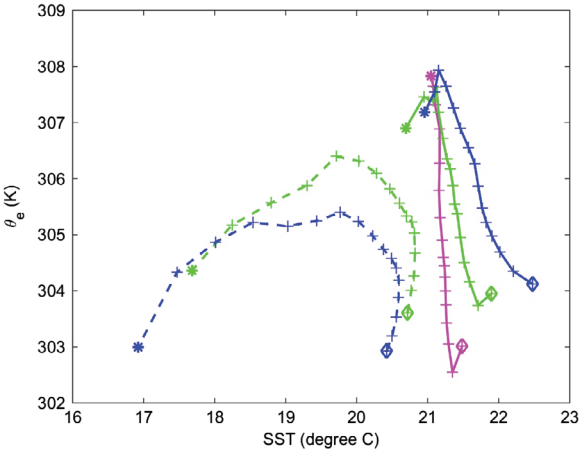

Fig. 5. Evolution of SST (x-axis, in deg °C) and θ_e (y-axis, in K) along the mean trajectories (CNTL, continuous lines; SMTH, dashed lines) from $t = 0$ h until the time their height exceeds that of the boundary layer. Values are given every hour (crosses) and the initial (final) location is indicated by a diamond (star). The same colour coding as in Fig. 3 is used.

between CNTL and SMTH (all colour subsets considered), the initial θ_e are comparable. Thus, the initial conditions do not favour a particular SST configuration with respect to θ_e (i.e. initial potential temperatures are not the largest for CNTL). The subsequent evolution however strikingly alters the θ_e of parcels. In the CNTL case (continuous curves), and in agreement with the thermodynamic mechanism, the SST changes only slightly while θ_e increases (y-axis). In the SMTH case however (dashed curves), the SST changes significantly (getting lower) while θ_e first increases but then decreases, with only a small net increase by the time the air parcels leave the boundary layer (this time is where the curves in Fig. 5 end, as indicated by a star – it was estimated from Fig. 4).

Why is this compensation occurring in SMTH? Inspection of Fig. 4b suggests that the decrease in θ_e in SMTH occurs when the parcels are getting close to the top of the boundary layer and are thus subject to a decrease in θ_e driven by entrainment of dry air from above (the vertical profiles of θ_e display a minimum just above the boundary layer at that time – not shown). A similar, although weaker, effect is seen in CNTL for the blue and green subsets and even less so for the magenta subset, in agreement with the fact that the boundary layer is higher up in CNTL than in SMTH (Fig. 4, dashed lines) and the fact that the magenta set is the closest to the sea surface in Fig. 4.

We conclude from this analysis that the thermodynamical mechanism explains well the contrast in number of trajectories between the CNTL and SMTH experiments, as the θ_e of air parcels at the time when they leave the boundary layer is several degrees lower in SMTH compared to CNTL (up to 5° C difference between the SMTH-blue subset and the CNTL-magenta subset). It is however more difficult to explain, based solely on

the value of θ_e acquired by air parcels at the time when they leave the boundary layer, how the small differences ($\approx 1\,^\circ$C) between the CNTL-magenta and CNTL-blue subsets in Fig. 5 (coloured star) could explain the very different heights reached subsequently at $t = 24$ h. Likewise, comparison of the blue and green subsets for CNTL and SMTH in Fig. 5, i.e. sets of trajectories reaching the same height, indicates large differences in θ_e (several degrees). Other effects are thus clearly important.

2.3.3. Dynamical analysis. To investigate further the dynamics, we display in Fig. 6 a comparison of the upward motion w at time $t = 24$ h and height $z = 4.5$ km between the CNTL and SMTH experiments. To do so, we have applied spatial low-pass and high-pass filters on the 12 km grid (these were simply obtained by averaging at each point the 10 neighbouring points – separated by approximately 12 km so overall an average over 240 km – in the zonal and meridional directions, the 'low-pass', and then removing this average, the 'high-pass'). The comparison of the low-pass fields (Fig. 6a for CNTL, Fig. 6b for SMTH, both shown in colour) indicates that the ascent near 70° W–37°N is more spatially spread out in SMTH than in CNTL, with a weaker magnitude. Even more striking are the high-pass filter fields (Fig. 6d for CNTL, Fig. 6e for SMTH) which show concentrated signals in CNTL but a more elongated and weaker distribution of updrafts/downdrafts in SMTH. This state of affair suggests that while there is always some form of convective motions developing along the front at 12 km resolution, these motions are more concentrated geographically and more intense in the CNTL experiment.

Analysis of the potential vorticity (PV) fields at the same time and height confirms this view (Fig. 7). There, we observe a more pronounced and intense region of negative PV in the CNTL experiment (Fig. 7a) compared to the SMTH experiment (Fig. 7b). In the context of symmetric flows, this is a known signature of inertial instability along isentropic surfaces (e.g. Bennetts and Hoskins, 1979, Emanuel, 1983, Thomas and Taylor, 2010). In the 3D flow considered here, we have checked that the high-pass correlations $\overline{u'w'}$ and $\overline{v'w'}$ in which u', v' refer to the high-pass zonal and meridional velocities, respectively, and in which the bar represents the low-pass average, tend to weaken the vertical shear of the flow (not shown) in CNTL but not in SMTH. This confirms the presence of some form of shear instability in CNTL at 12 km. A similar feature is present in COOL, but with a weaker magnitude of $\overline{u'w'}$ and $\overline{v'w'}$ (not shown). This is consistent with the fact that the statistics displayed in Table 1 for this experiment are somewhat intermediate between those in CNTL and SMTH. It is important to re-emphasize that while the SST gradients are exactly the same in CNTL and COOL, there is a drastic reduction in the number of trajectories reaching above 7 km in COOL (only 29 as opposed to 167 in CNTL). This suggests that the intensity of the instability is sensitive to the absolute value of SST but it is unclear at present how this is related to the thermodynamics arguments made in Section 2.3.2.

2.3.4. Summary. In summary, both the 'thermodynamical' and 'dynamical' mechanisms are acting constructively and are needed to explain the differences in upward motion between CNTL and SMTH. This likely reflects the particular geometry of the problem: trajectories of air parcels at low levels have a similar orientation to the warm tongue of the Gulf Stream which allows them to maintain high θ_e while flowing just above the ocean (less surface sensible cooling, more surface evaporation, less drying by entrainment at the top of the boundary layer) while, at the same time, the large SST gradients to the north of the warm tongue reinforce the thermally direct circulation at the front (and possibly leads to its instability).

2.4. Dependence on spatial resolution

We have repeated the CNTL, SMTH and COOL experiments (and the back trajectory analysis) at an horizontal resolution of 40 km rather than 12 km. As can be seen in the statistics summary in Table 1 (third and fourth columns), there is a large and systematic reduction in the number of trajectories feeding the ascent from low levels in all experiments when going from 12 to 40 km. Separate examination of the trajectories reaching above and below 5 km (i.e. trajectories whose initial position z_o at $t = 24$ h is above or below 5 km) indicates that in all experiments at 40 km resolution, the number of trajectories originating below 5 km is larger than that originating above this level. So the profiles in Table 1 go from 'top-heavy' to 'bottom-heavy' when degrading the resolution (the ratio above/below 5 km is explictly given in the last row of statistics for each experiment). As was discussed in Section 2.3, the 'bottom-heavy' situation only occurred in the SMTH experiment at 12 km resolution. The most dramatic illustration of the impact of resolution is the complete absence at 40 km resolution of trajectories originating above 7 km at $t = 24$ h, while such trajectories represented $29/625 = 5\%$ and $167/1178 = 14\%$ of the population for the COOL and CNTL experiments at 12 km, respectively.

The only difference between a given experiment at 12 and 40 km is atmospheric resolution,[4] as the SSTs are identical (Fig. 6, black contours, compare the SST in CNTL at 12 km in panels a,d with the SST in CNTL at 40 km in panels c,f). We have repeated the thermodynamic analysis in Fig. 5 for the CNTL and SMTH experiments at 40 km and found again that in the CNTL experiment, air parcels acquired a larger θ_e by the time they left the boundary layer than in the SMTH experiment (not shown). This shows that the thermodynamic mechanism can again explain the differences between CNTL and SMTH at 40 km resolution. Nevertheless, air parcels leaving the boundary layer in the CNTL experiment were found to have a θ_e only 1 °C lower at 40 km than their counterpart at 12 km (not shown). This agrees with the fact that a similar number of low-level trajectories ($z_o < 5$ km) are found in both CNTL experiments (see the ratio 40 km/12 km being unity in Table 1 for $z_o < 5$ km). It does not explain however why the number of trajectories with $z_o \geq 5$ km is

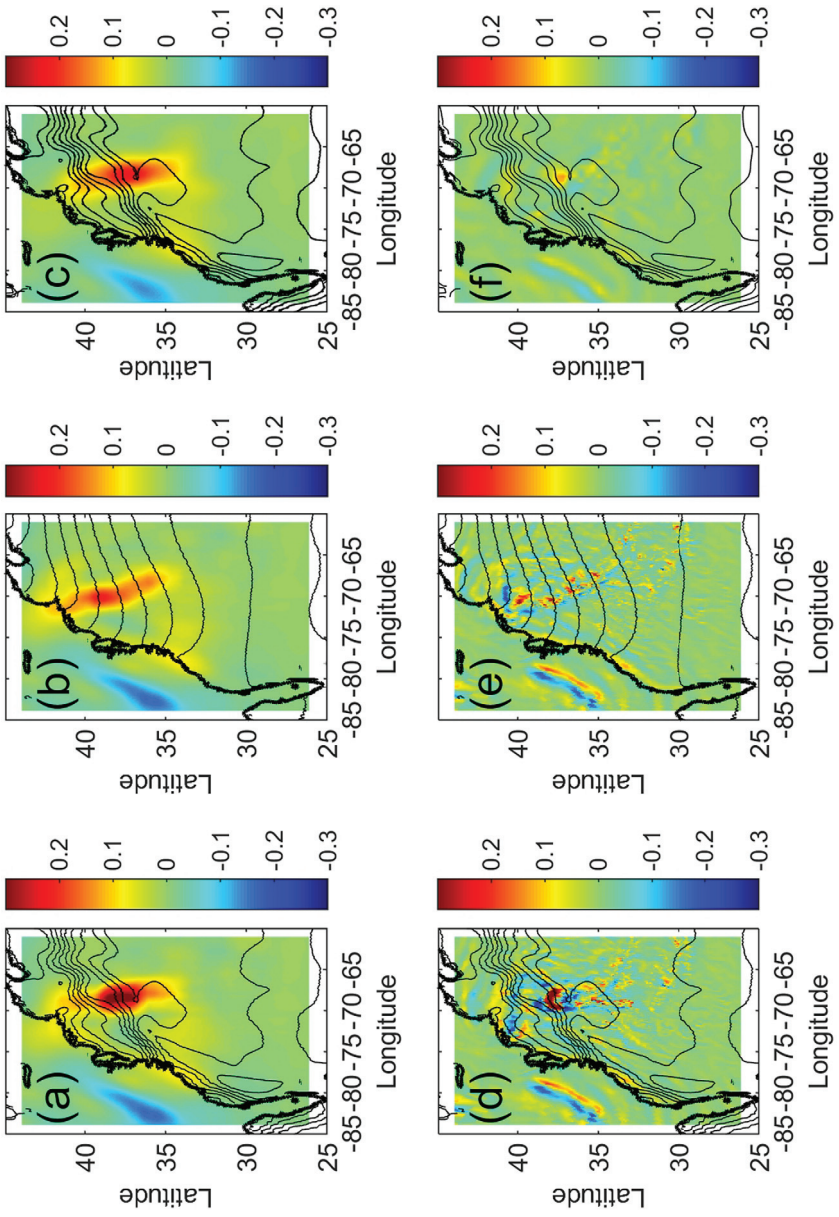

Fig. 6. Snapshots of vertical velocity at $t = 24$ h and a height of 4.5 km, decomposed into low-pass (panels a,b,c) and high-pass components (panels d,e,f) – see main text for details of the spatial filtering. The CNTL experiment is shown at 12 km resolution in panels (a,d) and at 40 km resolution in panels (c,f). The SMTH experiment at 12 km is shown in panels (b,e). The associated SST distributions are shown in black contours (same contouring as in Fig. 1).

reduced by more than a factor of two between these experiments (Table 1, ratio 40 km/12 km = 0.43).

To investigate further the dynamics, we have thus repeated the spatial filtering in Fig. 6 with the w field in CNTL at 40 km resolution (to do so we have first interpolated the 40 km fields onto the 12 km grid and then applied the spatial filters). The results are displayed in Fig. 6c (low-pass) and Fig. 6f (high-pass) and can be directly compared to the results for CNTL and SMTH at 12 km (Fig. 6a,c and Fig. 6b,e, respectively). The most striking feature is the absence of updrafts/downdrafts in the high-pass filtered fields in the 40 km case (not a priori ruled out by the 240 km width of the spatial filter) and the similarity between the low-pass fields for CNTL (40 km) and SMTH (12 km). The distribution of potential vorticity for CNTL (40 km) at $t = 24$ h and a height of 4.5 km in Fig. 7c shows a region of weakly negative PV ($PV \approx -0.2PVU$, $1PVU = 10^{-6}\,\mathrm{m^2\,K\,kg^{-1}\,s^{-1}}$), in contrast to the much lower values obtained in CNTL ($PV \leq -1PVU$, Fig. 7a). It is interesting that negative PV values of larger magnitude

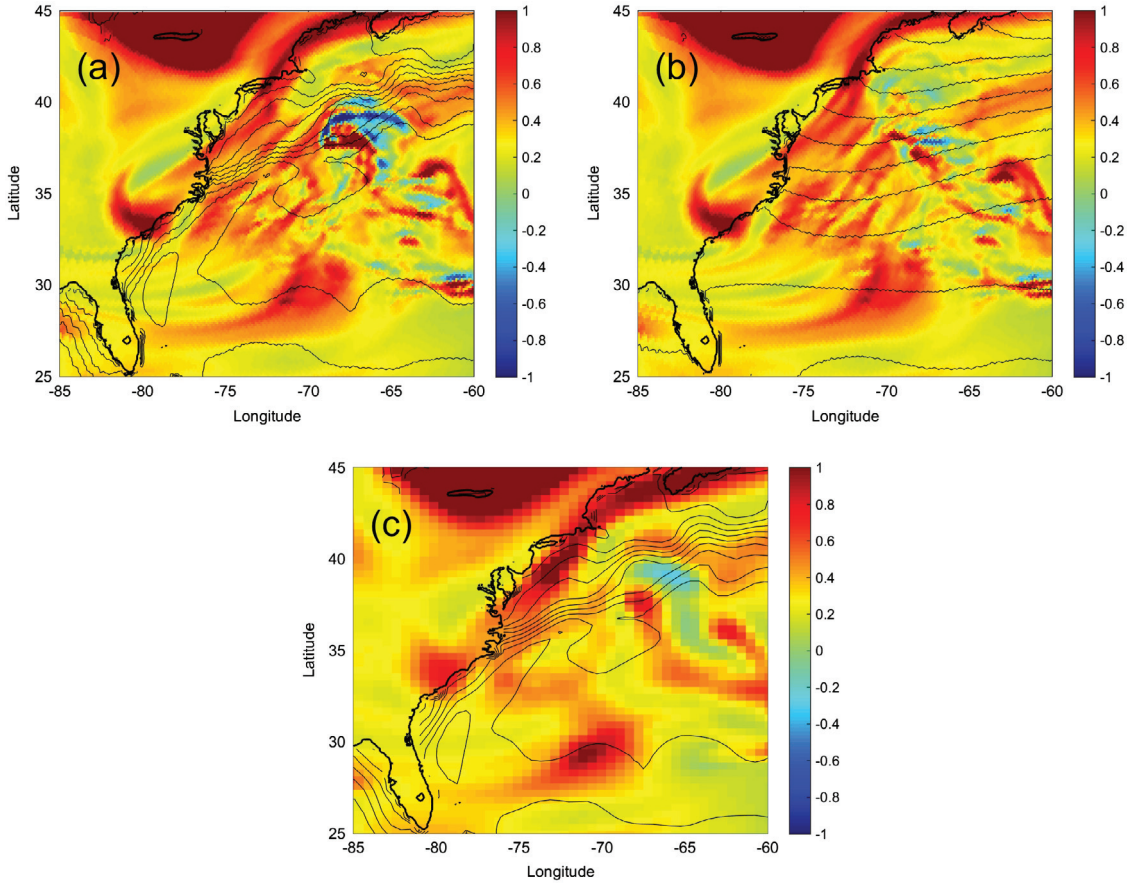

Fig. 7. Distribution of potential vorticity (in PVU, $1\,PVU = 10^{-6}\,\mathrm{m^2\,K\,kg^{-1}\,s^{-1}}$) at time $t = 24$ h and height $z = 4.5$ km. (a) CNTL at 12 km (b) SMTH at 12 km (c) CNTL at 40 km. The associated SST distributions are shown in black contours (same contouring as in Fig. 1).

are found in SMTH at 12 km (Fig. 7b) compared to CNTL at 40 km (but not in CNTL at 12 km), which suggests that the 40 km resolution is not able to maintain/generate low enough (negative) PV values. Overall, we conclude that the 40 km resolution is not able to capture the instability discussed in Section 2.3.2 when CNTL SST are prescribed and, as a result, cannot lead to deep ascent and the 'top heavy profiles' in Table 1.

3. Analysis of the ERA interim data-set

The previous section suggests that the Gulf Stream warm tongue has an impact on the ascending motion embedded in cyclones travelling in the northwest Atlantic, but it was only based on a single case study. To investigate whether this impact can also be detected in a climatological sense, we now analyse the ERA interim reanalysis data-sets over the 1979–2012 period (December through February). This data-set provides a gridded estimate of the state of the global atmosphere (here used on the native $T255$ truncation, approximately equivalent to a 80 km horizontal resolution) through a four-dimensional variational analysis and a 12-h analysis window (Dee et al., 2011). We do not expect the reanalysis data to capture the dynamics present in the simulations discussed in Section 2 because of its relatively coarse resolution. Our strategy is instead to use the ERA interim data to provide an estimate of the environment in which the smaller scale dynamics, and especially the enhanced ascent for air parcels flowing at low levels over the Gulf Stream warm tongue, might develop.

Specifically, we follow the framework of Shutts (1990), and compute trajectories along which enhanced ascent is expected to be found, given some environmental conditions. The trajectories in question are computed from the assumed conservation of the two components of absolute momentum (M and N) from an initial position at longitude λ_o and latitude ϕ_o. These components can be computed from:

$$M = 2\Omega \sin\phi a(\lambda - \lambda_o)\cos\phi + v, \tag{1}$$

$$N = 2\Omega a(\cos\phi - \cos\phi_o) - u \tag{2}$$

in which Ω is the Earth's rotation angular frequency, a is the Earth's radius, λ and ϕ denote longitude and latitude, respec-

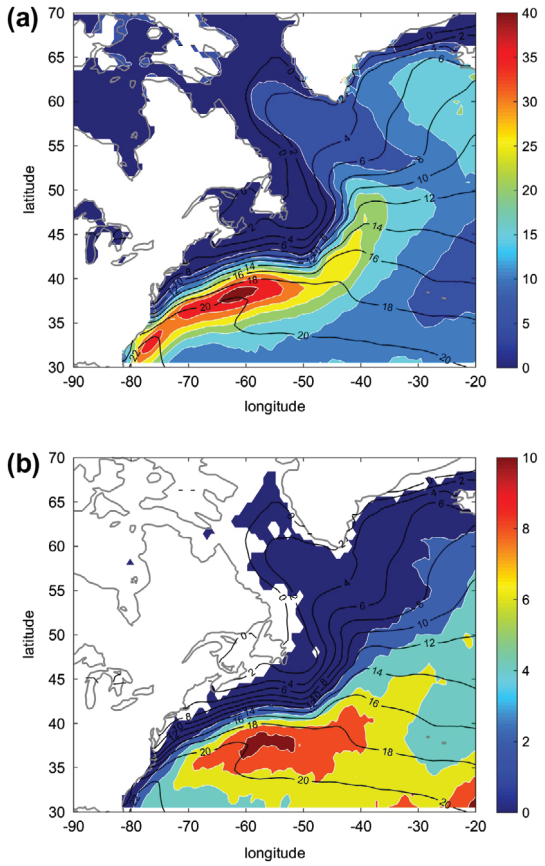

Fig. 8. Fraction of the time in winter (in %) when the condition $\Delta\theta_e > 0$ in eq. (3) is met for a surface θ_e (a) equal to an equilibrium value (b) equal to the actual θ_e at 950 hPa – see Section 3. The wintertime mean SST is displayed in black contours with a contour interval of 2 °C. All data from ERA interim in boreal winter. Note the factor of four difference between the colour bars in (a) and (b).

tively, and u and v are the zonal and meridional wind components, respectively. The assumption of conservation of M and N along the trajectory requires slow variations of the geostrophic flow in a particular direction, as occurs for example along a frontal region (Shutts, 1990). In addition, the method also assumes that the ascent occurs on a shorter timescale than the typical timescale of evolution of the system (Gray and Thorpe, 2001). Both assumptions are only approximately satisfied in the simulations discussed in Section 2 and in Nature so the results have to be treated with caution.

The calculation can be summarized as follows. At a given low-level grid point A (longitude λ_o, latitude θ_o) and time t_o, we compute the intersection of the M and N surfaces. This intersection defines a line as one moves upward, and we define point B as the intersection of this line with the tropopause (the latter was simply identified by the $2PVU$ contours, following Hoskins et al., 1985).[5] The difference $\Delta\theta_e$ in equivalent potential temperature θ_e between the two points represents a measure of the stability of the displacement:

$$\Delta\theta_e(\lambda_o, \phi_o, t_o) = \theta_e(A, t_o) - \theta_e(B, t_o) \tag{3}$$

If this quantity is positive, one can think that the buoyancy of the parcel at A is greater than that at B so an unstable and vigorous displacement can occur.[6] This situation is reminiscent of the results obtained in Section 2 when analysing the CNTL and COOL experiments ran at 12 km resolution. Our working hypothesis is thus that situations in which $\Delta\theta_e$ is positive should be found more frequently over the Gulf Stream warm tongue than over the surrounding waters.

To test this hypothesis, let us first consider the ideal scenario in which air parcels flowing over the Gulf Stream warm tongue are very nearly thermodynamically adjusted to the ocean. In that case, we can plausibly set $\theta_e(A, t_o)$ to be the equivalent potential temperature that an air sample would have if its temperature were equal to the SST and its relative humidity were equal to 80% (a typical value in the open ocean). The fraction of the time in winter when the condition $\Delta\theta_e > 0$ is met with this particular choice is shown in Fig. 8a. Strikingly, and in support of our hypothesis, one observes that occurrences are maximized along the Gulf Stream warm tongue, and much reduced elsewhere. Along the warm tongue, values as high as 40% are found.

The above calculation is clearly an overestimation since not all air streams at low levels are close to thermodynamic equilibrium with the ocean. To consider a more realistic situation, we thus set, in a second calculation, $\theta_e(A, t_o)$ to be the actual equivalent potential temperature at 950 hPa. The resulting map of occurrence is displayed in Fig. 8b. As expected, the magnitudes drop compared to Fig. 8a (note the factor of 4 difference in the colour bar between the two panels), but one still observes a clear maximum along the Gulf Stream warm tongue.

An interesting feature of the maps in Fig. 8 is that although the Gulf Stream extends significantly downstream of the region which we referred to as the warm tongue, it is the latter which is singled out in these maps. Very large heat exchanges occur throughout the path of the Gulf Stream but there is no indication in Fig. 8 that air parcels lifted from just above this ocean current can reach high vertical levels north of about 40°N. It is more likely that these air parcels are confined to the cold sector of the storms and that, as a result, the associated heat exchanges are confined to the maritime boundary layer. Indeed, the vertical motion is mostly downward in this part of the cyclones and this tends to restrict the vertical penetration of the oceanic influence there (e.g. Vannière et al., 2017).

In summary, application of a dynamical diagnostic to the environmental conditions provided by the ERA interim data suggests that the Gulf Stream warm tongue is the region where vigorous ascent from low levels should be most frequently observed in the Northwest Atlantic in winter. The occurrence of such events is comparable (5–10% of the wintertime based on Fig. 8b) to

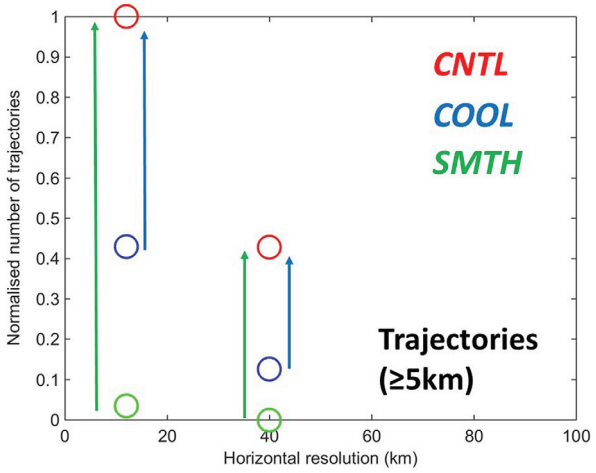

Fig. 9. Number of back-trajectories (circles) with heights $z \geq 5$ km at $t = 24$ h and reaching low levels over the ocean at $t = 0$ h (from Table 1 for all experiments): red for CNTL, blue for COOL and green for SMTH. The arrows indicate a measure of oceanic forcing when comparing CNTL/SMTH or CNTL/COOL (see main text). Note that the number of trajectories was normalized such that the number for CNTL at 12 km resolution is unity in order to facilitate the comparison between experiments.

that of the surface fronts detected over the Gulf Stream (e.g. Berry et al., 2011) so they must be an intrinsic feature of their dynamics in that region. This suggests that the modelling results obtained in Section 2 for a single case study have relevance to the climatological state in the North Atlantic. It is clear however that more case studies need to be analysed in order to settle this issue more firmly.

4. Summary and discussion

It has been known for many years that individual cyclones are sensitive to the distribution of SST in the Northwest Atlantic (e.g. Kuo et al., 1991; Reed et al., 1993; Booth et al., 2012). In addition, it is also well established that the climatological distribution of WCBs in the Northern hemisphere winter peaks over the Gulf Stream warm tongue (e.g. Madonna et al., 2014), and that phenomenona associated with vigorous updrafts such as lightning strikes are preferentially found over the Gulf Stream in winter (Christian et al., 2003). The novelty of our study is to suggest that these features are influenced by the particular geometry of air parcels' trajectories embedded in the cyclone at low levels and how these relate to the underlying SST distribution. Specifically, we proposed that the alignment of air parcels' trajectories at low levels with the Gulf Stream warm tongue and the associated SST gradients on its poleward flank are key to the enhancement, and perhaps the destabilization, of upward motion in cyclones travelling over the north-west Atlantic. It was further argued that both thermodynamical (absolute temperature of the warm tongue) and dynamical (strength of the SST gradient) effects were needed to produce this effect. While this conclusion was based on a single case study using high-resolution (12 km) simulations with the MetUM model, it was also supported by the application of a dynamical diagnostic to a climatological data-set (ERA interim reanalysis, 1979–2012, wintertime).

Our study raises an important question regarding the spatial resolution needed to simulate accurately the response of the atmosphere to the presence of the Gulf Stream and, more generally, the climatic impact of the extra-tropical oceans. To illustrate why resolution might be of importance, and building up on the results of Willison et al. (2013), consider the results of the back trajectory analysis in Section 2. It can reasonably be argued that the diabatic heating in the ascending branch of the simulated cyclone scales with the upward mass transport of this branch, as the diabatic heating results from the condensation of water vapour carried by the flow. In turn, we expect this upward mass transport to scale with the number of trajectories feeding the ascent. Under this assumption, the difference in the number of trajectories found under two different SST configurations provides a measure of oceanic forcing.[7] This idea is applied in Fig. 9 using the numbers in Table 1 for back-trajectories starting above 5 km at $t = 24$ h, in an attempt to estimate an upper level oceanic forcing. In this figure, we normalized the number of trajectories by that found in the CNTL experiment at 12 km (red circle on the left column). The green arrow indicates the normalized change in the number of trajectories when comparing a realistic (CNTL) and a smoothed (SMTH) SST distribution at 12 km (left column) or 40 km (right column) – likewise for the blue arrow and comparing realistic and colder SST anomalies (CNTL vs COOL). The length of the arrows, a plausible proxy for the strength of the oceanic forcing, is reduced by a factor of 2.2 (green) and a factor 1.9 (blue) at 40 km compared to 12 km.

The lower end of resolution considered in this study (40 km) is still much higher than that used in most climate models. An extrapolation of the results in Fig. 9 would suggest that upper level oceanic forcing associated with a smoothing of the SST gradient would be almost inexistent for grid sizes on the order of a few 100 km. A possible implication of our study is thus that climate models with grid sizes of several 100 km cannot simulate accurately the impact of the Gulf Stream warm tongue on the warm sector of cyclones (we refer to this impact as a 'warm path' for the oceanic influence). It is likely that this is the primary reason why the response of Atmospheric General Circulation Models (AGCMs) to extra-tropical SST anomalies has so far proven not to be robust (Kushnir et al., 2002). Indeed, AGCMs with grid sizes on the order of 100 km or more can only represent the shallow thermal forcing associated with air–sea interactions in the cold sector of cyclones (a 'cold path' to keep with the above terminology – see Vannière et al., 2017) and it is known that the response of the atmosphere to such heating is quite sensitive to the model background state (e.g. Ting and Peng, 1995; Kushnir et al., 2002). In contrast, the warm path

highlighted in our study consists of a modulation of the upward motion and latent heating (with, as emphasized in Section 1, a weak signature in the surface heat flux), and thereby represents a direct forcing of the upper levels heat and vorticity budgets. We thus expect this pathway of oceanic influence to be more robust. Recent experiments by Smirnov et al. (2015) suggest that as the horizontal resolution of an AGCM is increased from about 100 to 25 km, its response to the same SST anomaly becomes fundamentally different in character (from a weak to a strong upper level response). This, we suggest, could be the signature of the SST forcing switching from cold to warm path in this model.

Acknowledgements

Discussions with B. J. Hoskins are greatly acknowledged.

Disclosure statement

No potential conflict of interest was reported by the authors.

Funding

This work is part of Luke Sheldon's PhD funded by the Grantham Institute at Imperial College and in collaboration with the UK Met Office through a CASE studentship. Benoit Vannière is funded by the Natural Environment Research Council [grant number NE/J023760/1].

Notes

1. Although only shown here on a given day (14 January 2004), this feature persists in the climatological wintertime mean (not shown). The SST plotted in Fig. 1a is taken from the ECMWF operational analysis (25 km resolution) and interpolated on the 12 km grid of the MetUM model discussed below.
2. The North Atlantic domain has a non-uniform grid which is obtained by rotation of a uniform equatorial grid to the mid-latitudes (the typical grid point spacing being $\approx 0.1°$). It extends eastward from 20°E up to 70°E and westward from 7° W up to 120° W, depending on latitude (the latter itself ranges from as low as 10°N to as high as 80°N).
3. The equivalent potential temperature is computed in this study from $s = c_{p,d} \ln(\theta_e / T_{ref})$ in which $c_{p,d}$ is the specific heat capacity of dry air, $T_{ref} = 273.15\,\mathrm{K}$ and s is the specific entropy of moist air given by the approximate formula (Emanuel, 1994): $s = c_{p,d} \ln(T/T_{ref}) - R_d \ln(P_d/P_{ref}) + l_v q_v / T - R_v q_v \ln(RH)$. In this expression, R_d and R_v denote the gas constants for dry air and water vapour, respectively, P_d is the partial pressure of dry air, $P_{ref} = 1000\,\mathrm{hPa}$, l_v is the latent heat of vaporization, q_v is the specific humidity and RH is the relative humidity.
4. Note that the 40 km set-up has a *higher* vertical resolution with 38 levels between the sea surface and 10 km while there are 22 such levels for the 12 km set-up.
5. The idea is that tropospheric air has typically low values of PV, on the order of $1.5\,PVU$ or below, while stratospheric air has values in excess of $4\,PVU$. The choice of $2\,PVU$ allows to capture the transition, i.e. the tropopause.
6. This would be an exact statement in a purely two-dimensional flow (e.g. Emanuel, 1983) and is only an approximate statement in three dimensions.
7. This upper level forcing can be thought of as 'thermal' if phrased in terms of latent heat release as was just done. It can also be thought of as mechanical if it is considered from the point of view of the perturbed ascending motion – see Parfitt and Czaja (2016).

References

Bauer, M. and Del Genio, A. D. 2006. Composite analysis of winter cyclones in a GCM: Influence on climatological humidity. *J. Clim.* **19**, 1652–1672.

Bennetts, D. A. and Hoskins, B. J. 1979. Conditional symmetric instability, a possible explanation for frontal rain bands. *Quart. J. Roy. Met. Soc.* **105**, 945–962.

Berry, G. B., Reeder, M. J. and Jakob, C. 2011. A global climatology of atmospheric fronts. *Geopys. Res. Lett.* **38**(4), L04809.

Booth, J. F., Thompson, L., Patoux, J. and Kelly, K. A. 2012. Sensitivity of midlatitude storm intensification to perturbations in the sea surface temperature near the Gulf Stream. *Mon. Weather Rev.* **140**, 1241–1256.

Boutle, I., Belcher, S. E. and Plant, R. S. 2011. Moisture transport in midlatitude cyclones. *Q. J. R. Meteor. Soc.* **137**, 360–373.

Browning, K. A. 1990. Organization of clouds and precipitation in extratropical cyclones. In: *Extratropical Cyclones: The Erik H. Palmen Memorial Volume* (eds. C. Newton and E. Holopainen). American Meteor Society, Boston, pp. 129–153.

Catto, J. L., Shaffrey, L. C. and Hodges, K. I. 2010. Can climate models capture the structure of extratropical cyclones? *J. Clim.* **23**, 1621–1635.

Christian, H. J., Blakeslee, R. J., Boccippio, D. J., Boeck, W. L., Buechler, D. E., and co-authors. 2003. Global frequency and distribution of lightning as observed from space by the optical transient detector. *J. Geophys. Res.* **108**(D1), 4005. DOI: 10.1029/2002JD002347.

Czaja, A. and Blunt, N. 2011. A new mechanism for ocean-atmosphere coupling in mid-latitudes. *Q. J. R. Meteor. Soc.* **137**, 1095–1101.

Dee, D., Uppala, S. M., Simmons, A. J., Berrisford, P., Poli, P., and co-authors. 2011. The ERA-interim reanalysis: Configuration and performance of the data assimilation system. *Q. J. R. Meteor. Soc.* **137**, 553–597.

Eliassen, A. 1962. On the vertical circulation in frontal zones. *Geofys. Publ.* **24**, 147–160.

Emanuel, K. A. 1983. The lagrangian parcel dynamics of moist symmetric instability. *J. Atm. Sci.* **40**, 2368–2376.

Emanuel, K. A. 1994. *Atmospheric Convection*. Oxford University Press, Oxford.

Gill, A. E. 1982. *Atmosphere-Ocean Dynamics*, Academic Press, London, 1–662.

Gray, S. L. and Thorpe, A. J. 2001. Parcel theory in three dimensions and the calculation of SCAPE. *Mon. Wea. Rev.* **129**, 1656–1672.

Hoskins, B. J. and Karoly, D. 1981. The steady linear response of a spherical atmosphere to thermal and orographic forcing. *J. Atmos. Sci.* **38**, 1179–1196.

Hoskins, B. J., McIntyre, M. E. and Robertson, A. W. 1985. On the use and significance of isentropic potential vorticity maps. *Q. J. Roy. Meteor. Soc*. **111**, 877–946.

Hoskins, B. J. and Valdes, P. J. 1990. On the existence of storm-tracks. *J. Atmos. Sci*. **47**, 1854–1864.

Kuo, Y.-H., Reed, R. and Low-Nam, S. 1991. Effects of surface energy fluxes during the early development and rapid intensification stages of seven explosive cyclones in the western Atlantic. *Mon. Weather Rev.* **119**, 457–476.

Kushnir, Y., Robinson, W. A., Bladé, I., Hall, N. M. J., Peng, S., and co-authors. 2002. Atmospheric GCM response to extratropical SST anomalies: Synthesis and evaluation. *J. Clim*. **15**, 2233–2256.

Madonna, E., Wernli, H., Joos, H. and Martius, O. 2014. Warm conveyor belts in the ERA-interim dataset (1979–2010). Part I: Climatology and potential vorticity evolution. *J. Clim*. **27**, 3–26.

Manabe, S. and Stouffer, R. J. 1988. Two stable equilibria of a coupled ocean-atmosphere model. *J. Clim*. **1**, 841–866.

Martinez-Alvarado, O., Joos, H., Chagnon, J., Boettcher, M., Gray, S. L., and co-authors. 2014. The dichotomous structure of the warm conveyor belt. *Q. J. Roy. Meteor. Soc*. **140**(683), 1809–1824, Part B.

Parfitt, R. and Czaja, A. 2016. On the contribution of synoptic transients to the mean atmospheric state in the Gulf Stream region. *Q. J. Roy. Meteor. Soc*.. DOI: 10.1029/2011GL049573.

Pauluis, O., Czaja, A. and Korty, R. 2010. The global atmospheric circulation in moist isentropic coordinates. *J. Clim*. **23**, 3077–3093.

Reed, R. G., Greel, G. A. and Kuo, Y. 1993. The ERICA IOP 5 Storm: Analysis and simulation. *Mon. Weather Rev.* **121**, 1577–1594.

Shaman, R., Samelson, M. and Skyllingstad, E. 2010. Air-sea fluxes over the Gulf Stream region: Atmospheric controls and trends. *J. Clim*. **23**, 2651–2670.

Shutts, G. J. 1990. SCAPE charts from numerical weather model predictions fields. *Mon. Weather Rev.* **118**, 2745–2751.

Smirnov, D., Newman, M., Alexander, M. A., Kwon, Y. and Frankignoul, C. 2015. Investigating the local atmospheric response to a realistic shift in the Oyashio SST front. *J. Clim*. **28**, 1126–1147.

Thomas, L. N. and Taylor, J. R. 2010. Reduction of the usable wind work on the general circulation by forced symmetric instability. *Geophys. Res. Lett*. **37**, L18606. DOI: 10.1029/2010GL044680.

Ting, M. and Peng, S. 1995. Dynamics of early and middle winter atmospheric responses to northwest Atlantic SST anomalies. *J. Clim*. **8**, 2239–2254.

Vannière, B., Czaja, A., Dacre, H. and Woollings, T. 2017. A cold path for Gulf Stream–troposphere connection. *J. Clim* **30**, 1363–1379.

Willison, J., Robinson, W. A. and Lackmann, G. M. 2013. The importance of resolving mesoscale latent heating in the North Atlantic storm track. *J. Atmos. Sci*. **70**, 2234–2250.